Progress In Electromagnetics Research C, Vol. 106, 77–87, 2020

Compact Modified Hexagonal Spiral Resonator-Based Tri-Band Patch Antenna with Octagonal Slot for Wi-Fi/WLAN Applications

P. Rajalakshmi* and N. Gunavathi

Abstract—In this paper, a compact modified hexagonal spiral resonator-based tri-band patch antenna with an octagonal slot is presented for Wi-Fi/WLAN applications. The proposed antenna is designed on a low-cost FR4 substrate with a dielectric constant of $\varepsilon_r = 4.4$ and a loss tangent of $\delta = 0.02$. The tri-band operations have been achieved by a Modified Hexagonal Complementary Spiral Resonator (MHCSR) and an Octagonal slot. The loading of the MHCSR at the bottom of the substrate is to cover the 900 MHz (IEEE 802.11ah) band, and an Octagonal slot on top of the 5 GHz (IEEE 802.11a/h/j/n/ac/ax) rectangle patch is to cover the 2.4 GHz (IEEE 802.11b/g/n/ax) band. The prototype of the proposed antenna is fabricated and tested to validate the simulation results. The measured impedance bandwidth is 105 MHz at 900 MHz, 160 MHz at 2.4 GHz, and 180 MHz at 5 GHz. The designed antenna has a compact size with overall dimensions of $0.054\lambda_0 \times 0.066\lambda_0 \times 0.0048\lambda_0$ ($18 \times 22 \times 1.6\,\text{mm}^3$). The 82.2% reduction in size has been accomplished as compared to a conventional patch antenna at 900 MHz (lower resonance frequency). The waveguide setup method has been used to validate a negative permittivity property of the MHCSR. The parametric analysis of the proposed antenna has been carried out using the Ansoft HFSS19 software.

1. INTRODUCTION

With the rapid development of wireless communication technology, future systems need a very tiny antenna for recently introduced IEEE standards. The many standards of different frequency bands, such as Wi-Fi (IEEE 802.11a/b/g/h/n/ax)/WLAN (IEEE 802.11 j/ac) bands, CDMA800/GSM900 (IEEE 802.11 ah)/1800/1900 bands, are used for multi-band frameworks. Nowadays, to design a compact multi-band antenna, metamaterials are used. Metamaterials are artificial materials that do not exist in nature. Metamaterials exhibit various properties, such as negative permittivity and permeability. They are associated with antenna design and function, which leads to the enhancement of the antenna parameters such as bandwidth, efficiency, gain, and miniaturization [1, 2].

In [3–7], the compact dual-band antennas concentrate only on WLAN standards. In [8], a reflector metamaterial unit cell was demonstrated, making the dual-band operation at 5.7 GHz and 10.3 GHz with the large size of $35 \times 25 \times 0.787\,\text{mm}^3$. In [9], a microstrip antenna was designed by metamaterial with a fractal structure of poor impedance matching of −6 dB at 2.7 GHz. In [10], a slot antenna with SRR was designed for WLAN applications with a large size of $40 \times 40 \times 1.6\,\text{mm}^3$. The combination of a Split Ring Resonator (SRR) and an Electromagnetic Band Gap (EBG) with a fractal concept is used for antenna miniaturization with a complex structure, which resonates at 2.5 GHz and 5.9 GHz [11]. A low RCS circularly and linearly polarized slot antenna was designed only for dual-band operations by using an L-shaped copper strip and a CSRR-SRR array [12].

Received 18 August 2020, Accepted 23 September 2020, Scheduled 12 October 2020

* Corresponding author: Pitchai Rajalakshmi (rajalakshmipitchai10@gmail.com).

The authors are with the Department of Electronics and Communication Engineering, National Institute of Technology, Tiruchirappalli, Tamilnadu 620015, India.

In [13], a complicated cross-shaped patch antenna with a hexagonal CSRR array was proposed only to cover Wi-Fi applications. In [14], a complementary folded triangle split-ring resonator loaded dual-band patch antenna was designed for GSM1800 and Wi-Fi (IEEE 802.11 ax) applications. A complex structure of a dual-band CPW-fed metamaterial-inspired antenna was presented using the Composite Right/Left Handed (CRLH) metamaterial for Bluetooth, WLAN/Wi-Fi applications [15]. In [16], a modified split-ring resonator based short ended metamaterial antenna was discussed, which covered only Wi-Max applications. A coplanar waveguide fed planar antenna was proposed only to cover IEEE 802.11ac applications [17, 18]. The above mentioned already proposed antennas had obstacles such as large size or complex structure/design, and also they did not cover tri-bands. Hence, this work has been developed to fulfill the requirement of the society, such as the design of a compact, tri-band, low-cost planar antenna for the recently declared IEEE standards for Wi-Fi/WLAN applications.

This article demonstrates the loading of MHCSR that is enacted as a metamaterial with an octagonal slot on a rectangle patch antenna for GSM900 (IEEE 802.11ah) and Wi-Fi/WLAN (IEEE802.11a/b/g/h/j/n/ac/ax) applications. The use of MHCSR and octagonal slot makes the antenna size compact compared to a conventional microstrip patch antenna.

This article is written as follows. In Section 2, the antenna evolutionary stages and design specifications of the proposed antenna are presented. Section 3 address the design methodology of the octagonal slot and MHCSR. The negative permittivity extraction of the MHCSR metamaterial unit cell is explained in Section 4. Simulation and parametric analysis of the antenna are discussed in Section 5. The measured and simulated results of the designed antenna are given in Section 6.

2. ANTENNA EVOLUTIONARY STAGES AND DESIGN SPECIFICATIONS

The evolutionary stages of the designed antenna are depicted in Figure 1. Figure 2 shows the geometry of the designed antenna for Wi-Fi/WLAN applications. The designed antenna is fabricated on an FR4 substrate with a substrate thickness (h) of 1.6 mm. The designed antenna dimension is $0.054\lambda_0 \times 0.066\lambda_0 \times 0.0048\lambda_0$. 3D electromagnetic simulation software HFSS v.19 based on FEM is used for the simulation of the designed antenna. Initially, the rectangular patch antenna dimensions are computed by the equations in [19].

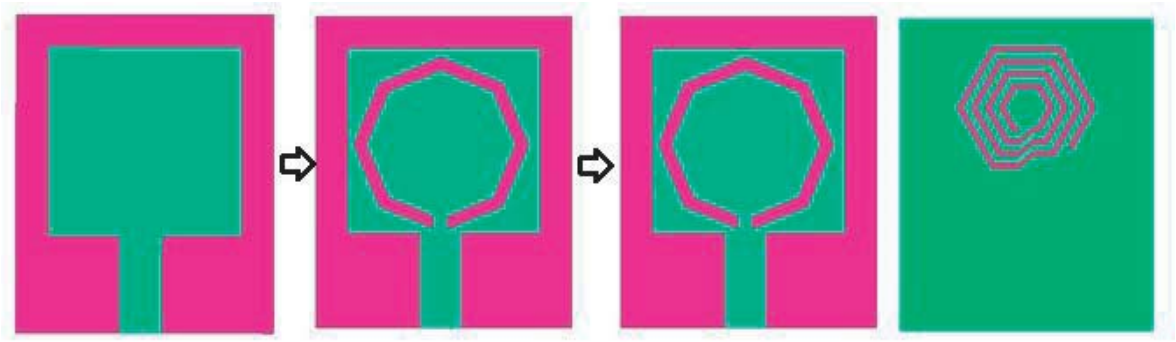

Figure 1. Design evolutionary stages of the designed antenna.

The proposed antenna's input port excitation is given through the 50 Ω characteristic impedance of a microstrip transmission line. Initially, a 5 GHz rectangle-shaped patch antenna is designed for single-band operation. The dual-band characteristics are at 2.4 GHz and 5 GHz, while an octagonal slot is introduced in the rectangular patch. Furthermore, MHCSR is loaded at the bottom of the ground plane to accomplish a new band at 900 MHz apart from two existing bands (2.4 GHz and 5 GHz). The optimized dimensions of the designed antenna (in mm) are given in Table 1.

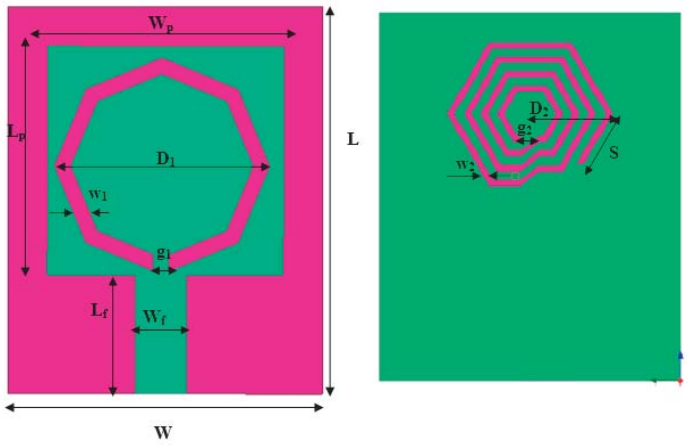

Figure 2. The geometry of the designed antenna.

Table 1. Optimized dimensions of the designed antenna.

Parameters	L	W	L_p	W_p	L_f	W_f	D_1
Dimensions in mm	22.0	18.0	13.0	13.5	6.75	2.9	12.2
Parameters	g_1	w_1	D_2	g_2	S	w_2	h
Dimensions in mm	0.9	1.0	5.0	1.0	2.25	0.5	1.6

3. OCTAGONAL SLOT AND MHCSR METAMATERIAL UNIT CELL DESIGN METHODOLOGY

The octagonal slot and MHCSR (metamaterial unit cell) are designed for 2.4 GHz and 900 MHz, respectively. These structures act as radiating elements within the rectangular patch, which are used for miniaturization.

3.1. Design Equations of the Octagonal Slot

The resonant frequency (f) of the octagonal slot is calculated by the following equations [1, 2].

$$f = \frac{c}{2l\sqrt{\varepsilon_{eff}}} \tag{1}$$

$$l = 8s - g_1 \tag{2}$$

l, s, and g_1 are the perimeter, side length, and split gap of the octagonal slot, respectively. c is the velocity of light. ε_{eff} is the effective permittivity of the substrate material.

3.2. Design Equations of the MHCSR Metamaterial Unit Cell

The resonant frequency (f) of the MHCSR metamaterial unit cell is calculated by the following equations [3–6]

$$L_{eq} = \frac{3\mu_0\mu_r}{2\pi}\left(\ln\left(\frac{S}{w}\right) - 1.405\right) \tag{3}$$

$$C_{eq} = 0.75SC_{pul} \tag{4}$$

$$C_{pul} = \frac{\sqrt{\varepsilon_{eff}}}{cZ_0} \tag{5}$$

$$f = \frac{1}{2\Pi\sqrt{L_{eq}C_{eq}}} \tag{6}$$

L_{eq} and C_{eq} are the total inductance and capacitance of the metamaterial unit cells, respectively. S and w are the sides of the MHCSR outer hexagonal length and width, respectively. C_{pul} and Z_0 are the capacitance per unit length between the rings and the medium's impedance, respectively. μ_0 and μ_r are the permeability of the free space and relative permeability of the medium, respectively.

4. NEGATIVE PERMITTIVITY EXTRACTION OF THE MHCSR METAMATERIAL UNIT CELL

The waveguide setup technique proposed by Chen et al. [20] is utilized to calculate the negative permeability and negative permittivity of the materials. z (Characteristic impedance) and n (Refractive Index) are computed by Equations (7) and (8), respectively [21]. Figure 3 demonstrates the waveguide setup created in HFSS to extract S_{21} and S_{11} of the proposed metamaterial resonator (MHCSR). In a waveguide setup, the Perfect Magnetic Conductor (PMC) and Perfect Electric Conductor (PEC) boundary are assigned in y- and x-directions, respectively. The electromagnetic wave is propagated in the z-direction.

$$z = \sqrt{\frac{(1+S_{11})^2 - S_{21}^2}{(1-S_{11})^2 - S_{21}^2}} \tag{7}$$

$$n = \frac{1}{kd}\cos^{-1}\left[\frac{1}{2S_{21}\left(1 - S_{11}^2 + S_{21}^2\right)}\right] \tag{8}$$

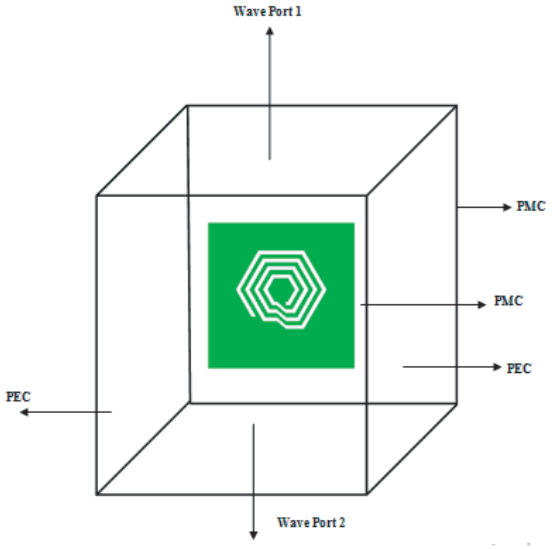

Figure 3. Simulation waveguide setup of the MHCSR metamaterial unit cell.

$$\varepsilon = \frac{n}{z} \tag{9}$$

where $k = 2\pi/\lambda$ is a wave number, and d is the slab thickness. The simulation-based S-parameters (S_{11} and S_{21}) representing the passband occurrence of the MHCSR at 900 MHz are portrayed in Figure 4. MATLAB code was written for Equations (7)–(9) to retrieve the negative permittivity characteristics of the MHCSR metamaterial unit cell structure from S_{11} (Reflection Coefficient) and S_{21} (Transmission Coefficient). The real part of the permittivity characteristics of the proposed metamaterial unit cell were found to be negative at 900 MHz, which suggests that MHCSR is a single negative substance containing the properties of the metamaterial, as shown in Figure 5.

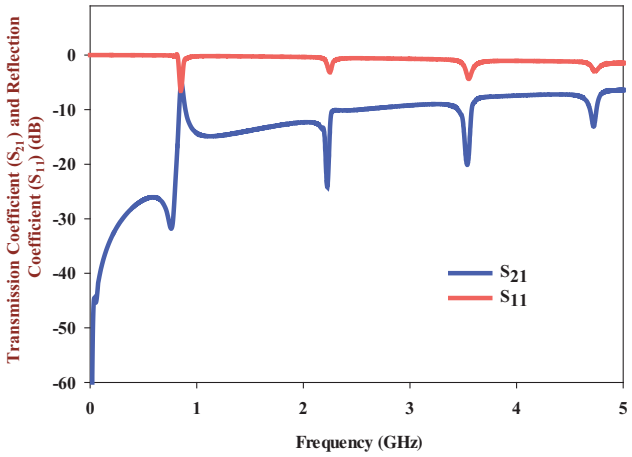

Figure 4. Frequency versus transmission and reflection coefficient plot of the MHCSR at 900 MHz.

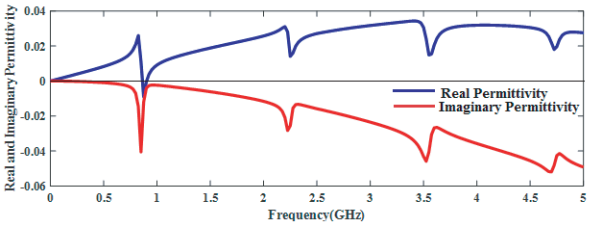

Figure 5. Frequency versus negative permittivity plot of the MHCSR at 900 MHz.

5. SIMULATION RESULT AND PARAMETRIC STUDY

From Figure 6, it is ascertained that a rectangle patch antenna produces a primary resonance frequency of 5.0 GHz. The introduction of this octagonal slot in the rectangular patch affects the patch's surface

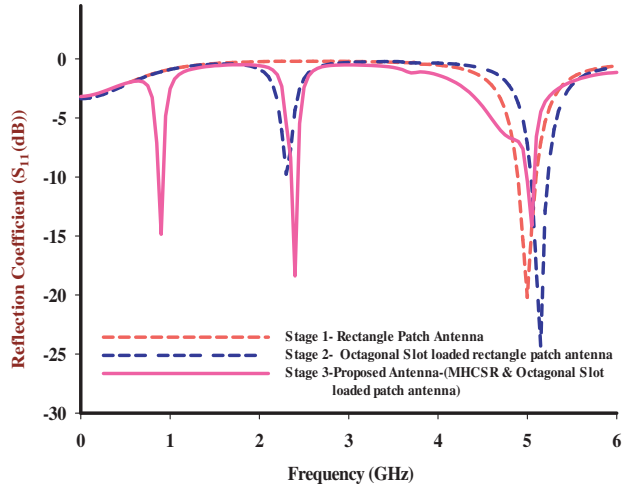

Figure 6. The simulated reflection coefficient characteristics of the evolutionary stages of the designed antenna.

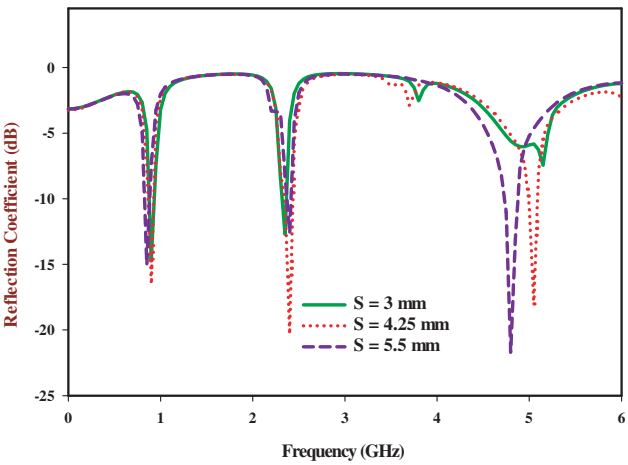

Figure 7. Simulated reflection coefficient characteristics for variation of S.

current distribution, consequently making a current supplement path for dual-band of operation. The octagonal slot-loaded radiating patch is combined into MHCSR to achieve tri-band resonances.

For the best results, a parametric study was done by using Ansoft HFSS19. The MHCSR metamaterial unit cell and octagonal slot parameters were controlled to tune the lower resonance (900 MHz) and middle resonance (2.4 GHz) frequencies of the designed antenna, respectively. As the side length (S) of the MHCSR decreases, the lower resonance frequency, as well as the higher resonance frequency of the designed antenna, decreases, and proper impedance matching is observed at $S = 4.25$ mm, as shown in Figure 7. Figure 8 shows that a decrease in g_1 decreases the middle resonance frequency. Figure 9 shows that a decrease in w_1 increases the middle resonance frequency of the antenna. The proper impedance matching is obtained at $g_1 = 0.9$ mm and $w_1 = 1$ mm. Based on the reflection coefficient plots, the MHCSR and octagonal slot parameters are optimized to achieve 900 MHz band and 2.4 GHz band, respectively.

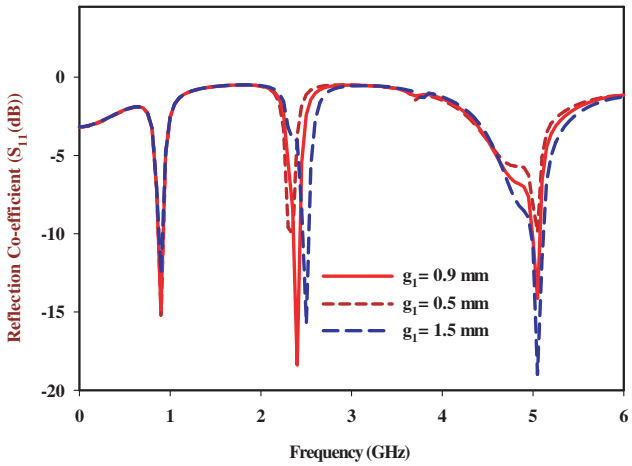

Figure 8. Simulated reflection coefficient characteristics for variation of g_1.

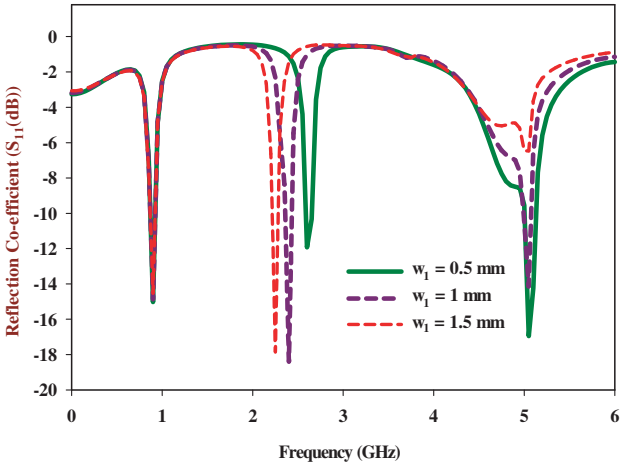

Figure 9. Simulated reflection coefficient characteristics for variation of w_1.

6. RESULTS AND DISCUSSION

The fabricated structure of the designed antenna is shown in Figure 10. The return loss of the designed antenna is estimated by utilizing Agilent PNA 8362B Vector Network Analyzer. The measured and simulated reflection coefficient characteristics of the designed antenna are exhibited in Figure 11, and the three resonance frequencies are obtained at 900 MHz, 2.4 GHz, and 5 GHz. As can be observed from Figure 11, the measured -10 dB impedance bandwidths are 105 MHz (842–947 MHz) at 900 MHz, 160 MHz (2.3–2.46 GHz) at 2.4 GHz, and 180 MHz (4.98–5.16 GHz) at 5 GHz, respectively.

The simulated and measured radiation patterns in the xz-plane ($phi = 0°$) and yz-plane ($phi = 90°$) for 900 MHz, 2.4 GHz, and 5 GHz are shown in Figures 12(a)–12(c), respectively. The results show

Figure 10. Photograph of the top view and bottom view of the proposed antenna.

that the designed antenna exhibits an omnidirectional radiation pattern in xy-plane for all resonant frequency bands. The dipole-like radiation pattern is at 900 MHz and 5 GHz resonant frequencies, with the directional radiation pattern at 2.4 GHz in the yz-plane. The small discrepancies observed in the simulated and measured results are due to soldering and fabrication errors.

The simulated surface current distribution at each resonant frequency band of the designed antenna is shown in Figure 13. At 5 GHz, the maximum current distribution flows in the rectangular patch of the antenna. The substantial concentration of the surface current at 2.4 GHz is observed in the feed position and ends of the octagonal slot of the antenna. The maximum current is distributed around the MHCSR at 900 MHz.

The simulated 3D gain plots of the designed antenna for all the resonance frequencies are shown in Figure 14. Figure 14 shows that the simulated 900 MHz and 5 GHz gains are 2.63 dB and 0.6 dB, respectively. The antenna achieves a simulated maximum peak gain of 10.9 dB at 2.4 GHz. Based on Table 2, the designed antenna has the best compactness and higher number of bands than [8, 11, 12–14, 16].

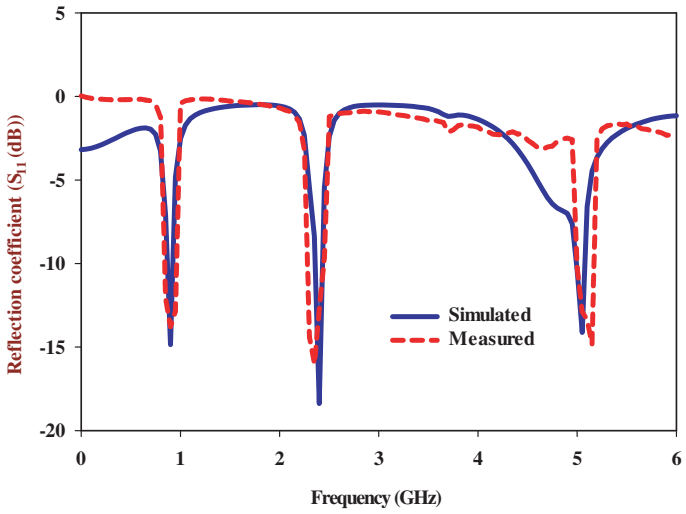

Figure 11. Simulated and measured reflection coefficient (dB) characteristics of the designed antenna.

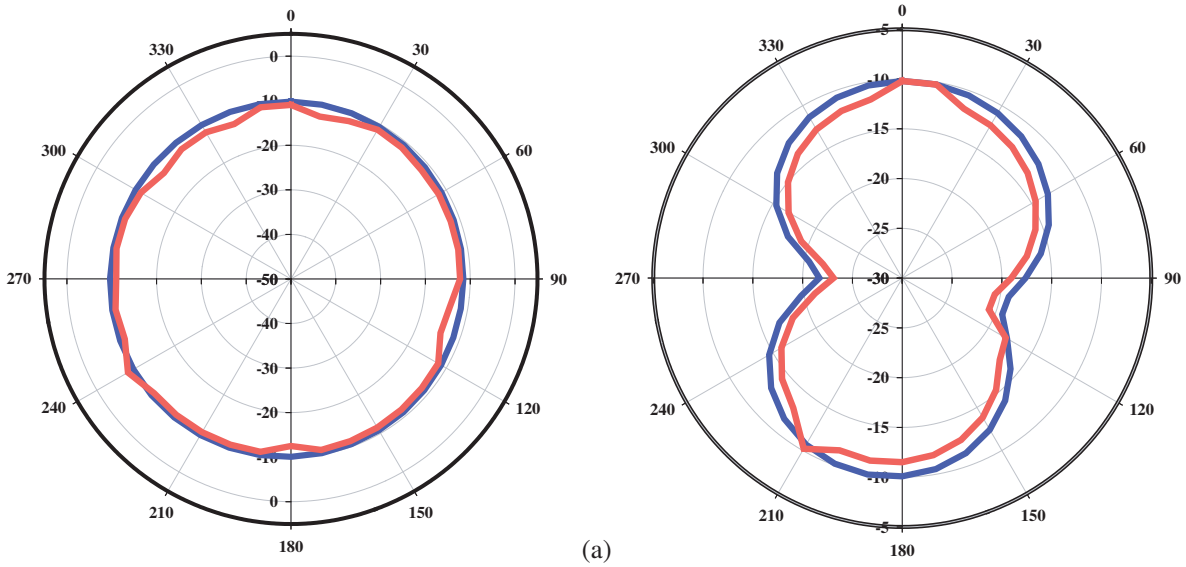

(a)

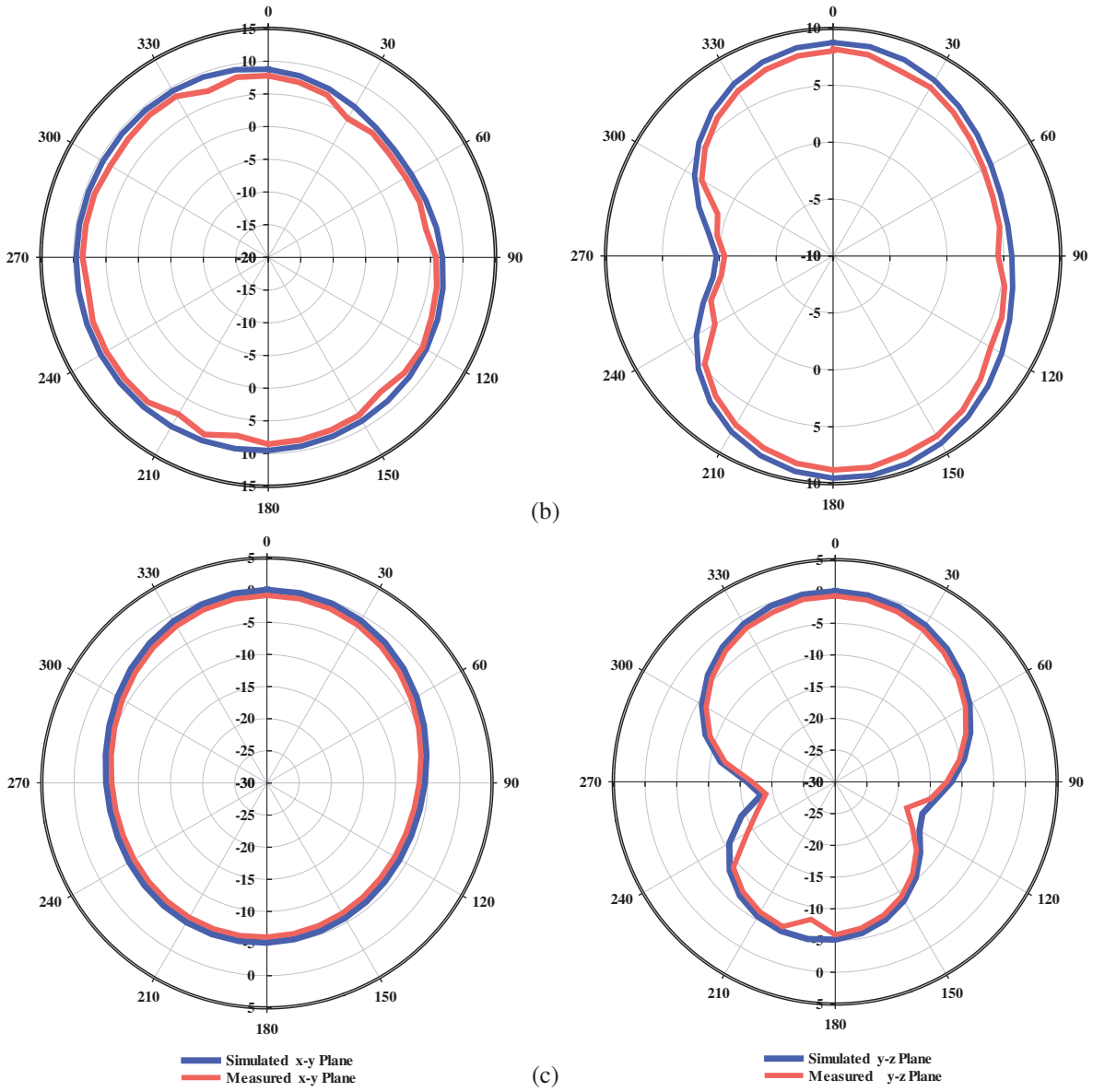

Figure 12. (a) Simulated and measured radiation pattern at 900 MHz. (b) Simulated and measured radiation pattern at 2.4 GHz. (c) Simulated and measured radiation pattern at 5 GHz.

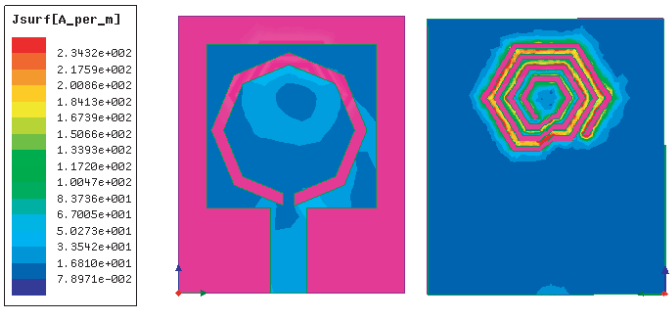

(a) 900 MHz

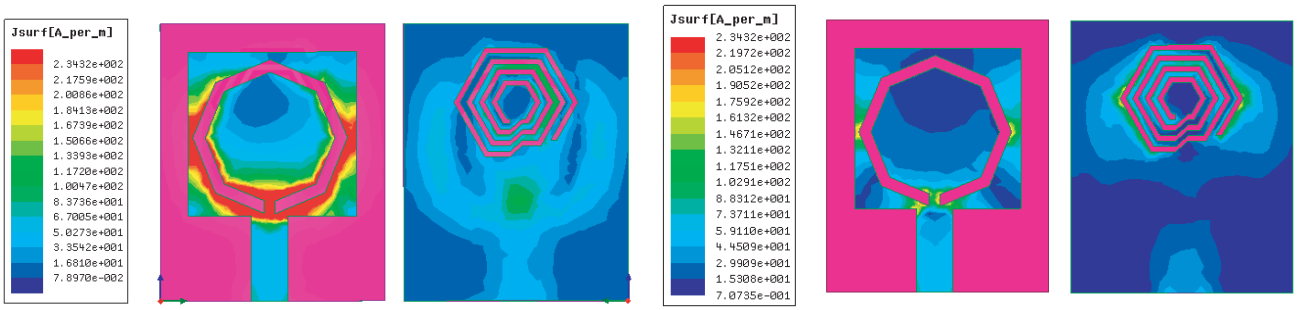

(b) 2.4 GHz (c) 5 GHz

Figure 13. Simulated surface current distribution of the designed antenna.

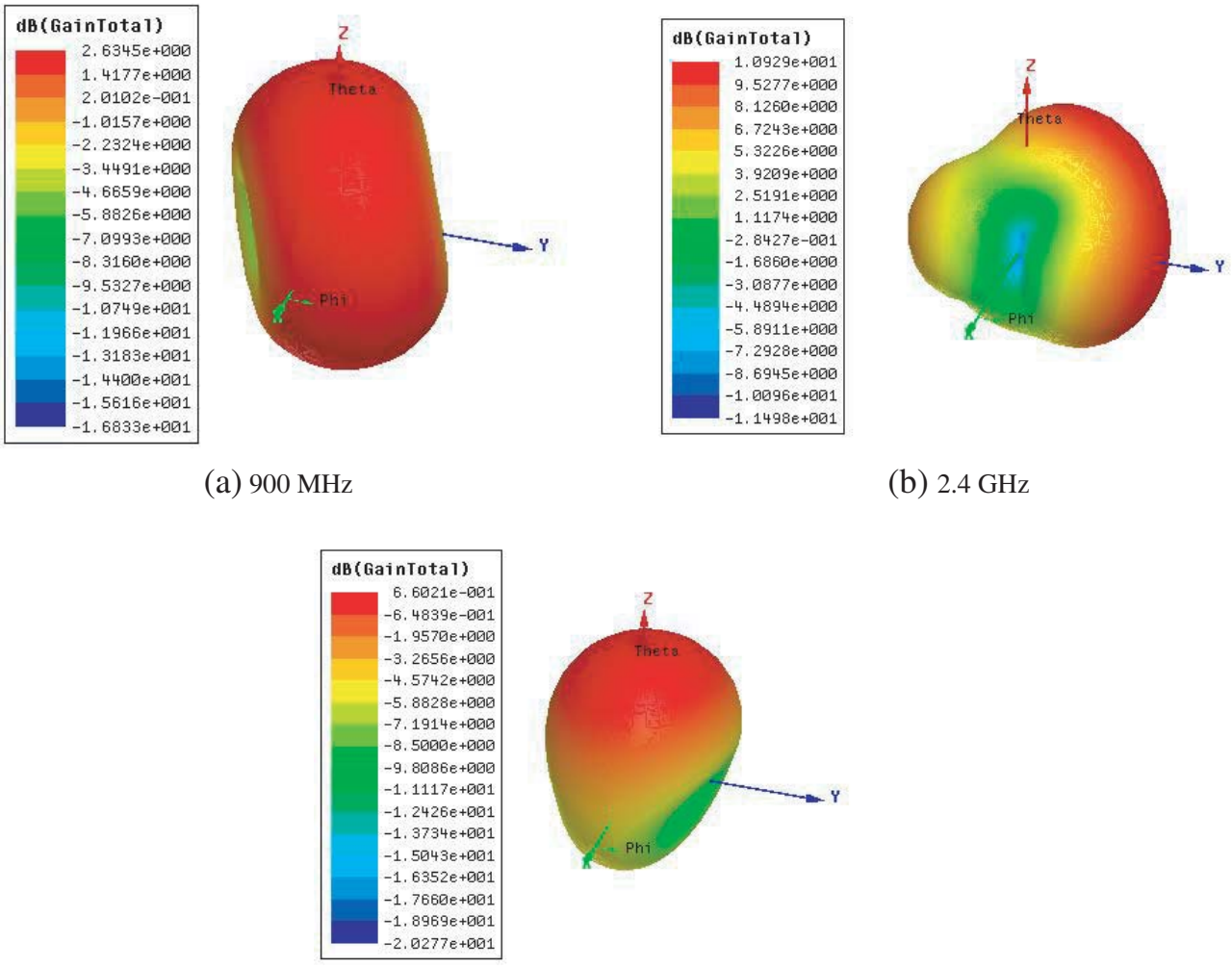

(a) 900 MHz (b) 2.4 GHz

(c) 5 GHz

Figure 14. Simulated 3D gain plot of the designed antenna.

Table 2. Comparison between the proposed antenna with existing antennas.

Reference	Year	Substrate material	Patch Dimensions $((W \times L \times h)\ \mathrm{mm}^3)$	Operational Bands	Frequency (GHz)
[8]	2019	RT Duriod	$35 \times 25 \times 0.787$	Dual-band	5.7/10.39
[11]	2017	FR4	$40 \times 40 \times 1.6$	Dual-band	2.5/5.9
[12]	2020	FR4	$50 \times 50 \times 1.56$	Dual-band	2.35/3.85
[13]	2018	FR4	$20 \times 25 \times 1.6$	Dual-band	2.4/5
[14]	2019	FR4	$16 \times 21 \times 1.6$	Dual-band	1.8/2.4/5
[16]	2017	FR4	$20 \times 25.5 \times 1.6$	Dual-band	3.17/5.39
Proposed		**FR4**	$\mathbf{18 \times 22 \times 1.6}$	**Tri-band**	**0.9/2.4/5**

7. CONCLUSION

A miniaturized tri-band MHCSR loaded patch antenna with an octagonal slot is designed, fabricated, and validated in this work. The proposed antenna exhibits tri-band operation at 900 MHz (842–947 MHz), 2.4 GHz (2300–2460 MHz), and 5 GHz (4980–5160 MHz), which meets the necessities of the recently introduced IEEE standards for the Wi-Fi/WLAN applications. The size reduction of 82.2% is achieved using an MHCSR metamaterial unit cell structure and octagonal slot. The metamaterial property is proved by using the negative permittivity plot of the MHCSR. The antenna characteristics such as proper impedance matching, multi-band operation, and compactness of the designed antenna make it suitable for the Wi-Fi/WLAN (IEEE 802.11a/b/g/h/j/n/ac/ax/ah) applications.

REFERENCES

1. Caloz, C. and T. Itoh, *Electromagnetic Metamaterials: Transmission Line Theory and Microwave Applications*, 1st Edition, Wiley-IEEE Press, Hoboken, NJ, ISBN-10: 0471669857, 2006.
2. Marque's, R., F. Martin, and M. Sorolla, *Metamaterials with Negative Parameters: Theory, Design and Microwave Applications*, Wiley, Hoboken, NJ, ISBN: 978-0-471-74582-2, 2007.
3. Huang, C. Y. and Yu. En-Zo, "A slot-monopole antenna for dual-band WLAN applications," *IEEE Antennas and Wireless Propagation Letters*, Vol. 10, 500–502, 2011.
4. Raj, R. K., M. Joseph, C. K. Aanandan, K. Vasudevan, and P. Mohanan, "A new compact microstrip-fed dual-band coplanar antenna for WLAN applications," *IEEE Transactions on Antennas and Propagation*, Vol. 54, No. 12, 3755–3762, 2006.
5. Malik, J., A. Patnaik, and M. V. Kartikeyan, "A compact dual-band antenna with omnidirectional radiation pattern," *IEEE Antennas and Wireless Propagation Letters*, Vol. 14, 503–506, 2015.
6. Chakraborty, U., A. Kundu, S. K. Chowdhury, and A. K. Bhattacharjee, "Compact dual-band microstrip antenna for IEEE 802.11a WLAN application," *IEEE Antennas and Wireless Propagation Letters*, Vol. 13, 407–410, 2014.
7. Peng, L. and C.-L. Ruan, "A microstrip fed Patch antenna with two parasitic invert L stubs for dual-band WLAN applications," *Wireless Personal Communications*, Vol. 57, 727–734, 2011.
8. Rajak, N., N. Chattoraj, and R. Mark, "Metamaterial cell inspired high gain multiband antenna for wireless applications," *International Journal of Electronics and Communications (AEU)*, Vol. 109, 23–30, 2019.
9. Varamini, G., A. Keshtkar, and M. Naser-Moghadasi, "Miniaturization of a microstrip loop antenna for wireless based on metamaterial metasurface," *International Journal of Electronics and Communications (AEU)*, Vol. 83, 32–39, 2018.

10. Pirooj, A., M. Naser-Moghadasi, and F. B. Zarrabi, "Design of compact slot antenna based on split ring resonator for 2.45/5 GHz WLAN applications with circular polarization," *Microwave and Optical Technology Letter*, Vol. 58, No. 1, 12–16, 2016.
11. Sedghi, M. S., M. Naser-Moghadasi, and F. B. Zarrabi, "Microstrip antenna miniaturization with fractal EBG and SRR loads for linear and circular polarization," *International Journal of Microwave and Wireless Technologies*, Vol. 9, No. 4, 891–901, 2017.
12. Hrideshkumarverma, R., S. Meena, M. Kumar, and S. P. Singh, "A low RCS compact circularly polarized dual band slot antenna loaded with SRR and CSRR for satellite applications," *International Journal of Electronics*, 2020, DOI: 10.1080/00207217.2020.1756436.
13. Rajalakshmi, P. and N. Gunavathi, "Gain enhancement of cross shaped patch antenna for IEEE 802.11ax Wi-Fi applications," *Progress In Electromagnetics Research Letters*, Vol. 80, 91–99, 2018.
14. Rajalakshmi, P. and N. Gunavathi, "Compact complementary folded triangle split ring resonator triband mobile handset planar antenna for voice and Wi-Fi applications," *Progress in Electromagnetics Research Letters*, Vol. 91, 253–264, 2019.
15. Gupta, A. and R. K. Chaudhary, "A compact dual-band short ended metamaterial antenna with extended bandwidth," *International Journal of RF and Microwave Computer-Aided Engineering*, Vol. 26, No. 5, 435–441, 2016.
16. Kukreja, J., D. K. Choudhary, and R. K. Chaudhary, "CPW fed miniaturized dual-band short ended metamaterial antenna using modified split ring resonator for wireless applications," *International Journal of RF and Microwave Computer-Aided Engineering*, Vol. 27, No. 8, 1–7, 2017.
17. Gunavathi, N. and D. Sriram Kumar, "CPW-fed monopole antenna with reduced radiation hazards towards human head using metallic thin-wire mesh for 802.11ac applications," *Microwave and Optical Technology Letters (MOTL)*, Vol. 57, No. 11, 2684–2687, 2015.
18. Gunavathi, N. and D. Sriram Kumar, "Miniaturized unilateral coplanar waveguide-fed asymmetric planar antenna with reduced radiation hazards for 802.11ac applications," *Microwave and Optical Technology Letters (MOTL)*, Vol. 58, No. 2, 338–343, 2015.
19. Balanis, C. A., *Antenna Theory: Analysis and Design*, John Wiley & Sons, New York, 2016.
20. Chen, H. J., J. Zhang, Y. Bai, Y. Luo, J. Q. Ran, et al., "Experimental retrieval of the effective parameters of metamaterial based on a waveguide method," *Optics Express*, Vol. 14, No. 26, 12944–12949, 2006.
21. Smith, D. R., S. Schultz, P. Markos, and C. M. Soukoulis, "Determination of negative permittivity and permeability of metamaterials from reflection and transmission coefficients," *Phys. Rev. B*, Vol. 65, No. 19, 2002.